ISSN 0915-633X

NATIONAL INSTITUTE FOR FUSION SCIENCE

An Estimation of Life Time for A Low Energy Negative Pionlike Particle Beam

J. Uramoto

(Received - Apr. 7, 1995)

NIFS-351 Apr. 1995

RESEARCH REPORT
NIFS Series

NAGOYA, JAPAN

An Estimation of Life Time for a Low Energy Negative Pionlike Particle Beam

Jōshin URAMOTO

National Institute for Fusion Science

Nagoya 464-01, Japan

Abstract

A life time of the negative pionlike particle beam which is produced by a low energy (< 1000 eV) electron bunch and positive ion bunch, is estimated from a flight time of the negative pionlike particle beam within a magnetic mass analyzing region and a reduction of the beam current during the flight time. We estimate that the life time is near the typical value 2.6×10^{-8} sec of the true negative pion.

Keywords: negative pionllike particle π^-, flight time, life time

1. Introduction

We have already reported[1] the following experimental facts. When a low energy electron beam (≤ 1200 eV) is injected perpendicularly to a uniform magnetic field, together with a low energy positive ion beam which is stopped electrically and the uniform magnetic field is used as a mass analyzer, two peaksof negative current to the beam collector appear at two analyzing magnetic field intensities which correspond to two relations of negative muon (the mass $m_1 = 207\ m_e$ and the charge $q_1 = e$) and negative pion (the mass $m_2 = 273\ m_e$ and the charge $q_2 = e$, where m_e and e are mass and charge of electron) Then, their life times should be estimated in order to compare with the typical life times $\tau_\mu = 2.2 \times 10^{-6}$ sec for the negative muonlike particle and $\tau_\pi = 2.6 \times 10^{-8}$ sec for the negative pionlike particle. In this report, the life time of the negative pionlike particle π^- will be estimated from flight times of π^- which are controlled by the effective acceleration voltages.[1]

2. Basic Experimental Conditions

Schematic diagrams of the basic experimental apparatus are shown in Fig. 1 and Fig. 2. The initial or first electron beam (F.E.B.) is stopped critically in front of the entrance slit S by an electrical potential of the decelerator D connected to the cathode of the electron gun. Next, a neutral gas is introduced into the first electron beam region and a plasma is produced through ionization of the gas. Then, positive ions of the plasma are accelerated in front of S while a positive ion beam with an energy corresponding to the first electron beam acceleration voltage V_A, is injected into the magnetic field region through S. Moreover, the stopped beam electrons are reaccelerated electrically toward the gap between two magnetic poles (N) and (S) through S, while the injected ion beam is decelerated electrically and stopped in the gap. The electrically reaccelerated electrons are injected perpendicularly to the magnetic field (B_M) and bunched in cyclotron motions of small radius.

As shown in Fig. 2, the above magnetic system is used as a mass analyzer (M.A.) of 90° type when the beam collector B.C. is arranged. The analyzing curvature radius r is 4.3 cm. It should be noted that the bias voltage V_S of the beam collector is positive with respect to the mass analyzer in order to measure a negative charge current.

A fringe magnetic field distribution of the analyzing magnetic field B_M under a magnetic coil current of 1A, is shown in Fig. 3 for two different metal plates as the entrance plate (decelerator D) of Fig. 1 and Fig. 2. The iron (Fe) plate is used and the fringe magnetic field is much reduced.

The distribution of electrically applied potential are shown in Fig. 4. The first electron beam from the electron gun is perfectly reflected in front of the entrance slit S of the magnetic mass analyzer (M.A.) while a plasma is produced by a gas (air) ionization. Then, a positive ion beam is injected into M.A. through the slit S and the second electron beam is produced by reacceleration of the plasma electrons. It should be noted that the injected positive ion beam (i_2) is decelerated and stopped electrically, and that the second electron beam (e_2) suffers a magnetron (cyclotron) motion in the uniform magnetic field (which is used as the analyzing magnetic field of M.A.). As a result, both the electron beam and positive ion beam will be bunched within the small space at the entrance X of the uniform magnetic field. As reported already,[1] we consider that a negative muonlike μ^- and a negative pionlike π^- particle beams are produced by a coherent interaction between the bunched electrons and positive ions. Because we find that the mass analyzing relations of negative muon and negative pion are satisfied for two peaks of negative current I^- to the beam collector B.C., if we assume that the effective acceleration voltage V_E is twice of the first electron beam acceleration voltage V_A. That is, the following relation is found: From the analyzing magnetic field B_M where the negative current shows a peak, the curvature radius r of the mass analyzer and the effective acceleration voltage V_E, we can estimate the mass m of the negatively charged particle by,

$$m = \frac{Ze\,(B_M r)^2}{2V_E}$$

$$= \frac{8.8 \times 10^{-2}\, Z\,(B_M r)^2\, m_e}{V_E}, \quad \text{..... (1)}$$

where e is the electron charge, B_M is in gauss unit, r is in cm unit, V_E is in volt unit and m_e is the electron mass and Z is the charge number. For the curvature radius $r = 4.3$ cm of this mass analyzer, the Eq. (1) is rewritten by

$$m = \frac{1.63\, Z\, B_M^2}{V_E} m_e \quad \text{..... (2)}$$

In the experiments as reported already,[1] we obtain $m = m_1 \approx 206\ m_e$ for the first peak of I^- and $m = m_2 \approx 290\ m_e$ for the second peak of I^-, assuming that $Z = 1$ and $V_E = 2\ V_A$.

3. Experiment for Estimation of Life Time

An experiment to estimate the life time of muonlike particle μ^- or pionlike particle π^- is tried by the experimental apparatus as shown in Fig. 2. In Fig. 5, dependences of a negative current I^- to the beam collector B.C. on the analyzing magnetic field B_M are shown for the first electron beam acceleration voltages ranging from $V_A = 100V$ to $V_A = 400V$. In their dependences, two kinds of peaks of the negative current I^- for the various voltages V_A, are seen, which correspond to the negative muonlike particle μ^- beams or pionlike particle π^- beams as related with Eq. (2), assuming that $V_E = 2\ V_A$. Besides, we must pay attention to variations of I^- for V_A. The two peak values of I^- corresponding to μ^- and π^- beam currents decay abruptly when the first electron acceleration voltage V_A decreases. That is, when V_A decreases from 400V to 100V, each peak value of I^- decreases about 1/17, while the variation for the peak value of electron beam current I_e near $B_M \approx 0$ is kept within about 1/2.5. We confirm experimentally that the above features on V_A do not vary for the first electron beam currents ($50\ \mu A \leq I_A \leq 0.5$ mA) where space charge effects do not become serious, and for differences between Air (8×10^{-6} Torr ~ 1.5×10^{-4} Torr) and Ar gas (2×10^{-5} Torr ~ 2×10^{-4} Torr) in the gas introduction region (G of Fig. 2).

4. Discussion

Each flight time of μ^- or π^- particles from the generation point X (in Fig. 2) to the beam collector B.C., is estimated by,

$$T_1 = \frac{\pi}{2} \frac{r}{v_1}$$

$$T_2 = \frac{\pi}{2} \frac{r}{v_2}, \quad \text{..... (3)}$$

where T_1 or T_2 is a flight time of μ^- or π^- particles, v_1 or v_2 is a mean velocity of μ^- or π^- particle and r is the mass analyzing radius (r = 4.3 cm). The mean velocities v_1 or v_2 are determined by the effective acceleration voltages $V_E = 2\ V_A$ (assuming the acceleration mechanism of Fig. 4). That is, in cm/sec unit,

$$v_1 = \sqrt{(\frac{2e}{m_1})(2\ V_A)} = 5.8 \times 10^6 \sqrt{V_A}$$

$$v_2 = \sqrt{(\frac{2e}{m_2})(2\ V_A)} = 5.1 \times 10^6 \sqrt{V_A}, \quad \text{..... (4)}$$

where m_1 is the mass of μ^- (= 207 m_e), m_2 is the mass of π^- (= 273 m_e) and V_A is in volt unit.

If the life time of μ^- or π^- particles is expressed by τ_μ or τ_π, the initial μ^- or π^- beam current I_{01}^- or I_{02}^- at the generating point X (in Fig. 2) is reduced on the way to the beam collector B.C., by

$$I_1^- = I_{01}^- \exp(-T_1/\tau_\mu)$$

$$I_2^- = I_{02}^- \exp(-T_2/\tau_\pi). \quad \text{..... (5)}$$

As well known, the typical τ_μ or τ_π has been estimated by

$$\tau_\mu \approx 2.2 \times 10^{-6} \text{ sec}$$

$$\tau_\pi \approx 2.6 \times 10^{-8} \text{ sec.} \quad \text{..... (6)}$$

From Eqs. (3), (4), (5) and (6), we obtain

$$\alpha_1 = I_1^-/I_{01}^- = \exp(-5.3 \times 10^{-1}/\sqrt{V_A})$$

$$\alpha_2 = I_2^-/I_{02}^- = \exp(-5.1 \times 10/\sqrt{V_A}), \quad \text{..... (7)}$$

where, α_1 or α_2 shows a reduction ratio of μ^- or π^- beam current.

For our experimental conditions $100V \leq V_A \leq 400V$, we obtain, from Eq (7),

$$1/1.06 \leq \alpha_1 \leq 1/1.03$$

$$1/164 \leq \alpha_2 \leq 1/13. \quad \ldots\ldots (8)$$

Here, if Eqs. (7) and (8) are normalized by a value of Γ^- at $V_A = 400V$, Eqs. (7) and (8) are rewritten by

$$\alpha_1' = 1.03\,\alpha_1$$

$$\alpha_2' = 13.0\,\alpha_2, \quad \ldots\ldots (7)'$$

$$1/1.03 \leq \alpha_1' \leq 1$$

$$1/13 \leq \alpha_2' \leq 1 \quad \ldots\ldots (8)'$$

To compare with experimental reduction ratios α_1' (Exp) and α_2' (Exp) with the theoretical reduction ratios α_1' (Th) and α_2' (Th) from Eq. (7)', we show Table 1, where all α_1' and α_2' are normalized by a value of Γ^- at $V_A = 400$. As understood from Table 1, we can not explain their reductions of Γ^- peaks in Fig. 5, from the life time of μ^- particles τ_μ. On the other hand, we can explain roughly, from the life time of π^- particles τ_π. That is, from Table 1, we find the following relation

$$0.5 < \frac{\alpha_1'\,(\mathrm{Th})}{\alpha_2'\,(\mathrm{Exp})} < 1.3, \quad \ldots\ldots (9)$$

which means that the experimental decay time constant of π^- particles is very near the typical life time τ_π. Consequently, we may consider that μ^- particles are produced secondly from the decay of π^- particles.

Reference

1. J. Uramoto, *NIFS Report* No. 277 (1994).

Fig. 1 and Fig. 2: Schematic diagrams of the basic experimental apparatus.

F: Filament as electron emitter. K. Cathode of electron gun. A: Anode of electron gun. V_A: Initial electron acceleration voltage. I_A: Total negative current. F.E.B.: First electron beam. G: Neutral gas. D: Decelerator of F.E.B. S: Entrance slit (3 mm × 10 mm). Ins. Insulator. I.B.: Ion beam. S.E.B.: Second electron beam. e: Electrons with cyclotron motions. μ^-: Negative muonlike particle. (M.A.): Mass analyzer. Fe: Iron. C: Magnetic Coil. (N): North pole of electro-magnet. (S): South pole. B_M: Analyzing magnetic field. B.C.: Beam collector. I^-: Negative current to B.C. V_S: Bias voltage of B.C. with respect to mass analyzer body. S.P.: Secondary plasma generating outside the mass analyzing region. X: Entrance of uniform magnetic field. i: Ion bunch. π^-: Negative pionlike particle. The neutral gas (air) pressure is about 3×10^{-6} Torr in the electron gun region and 1×10^{-5} Torr in the plasma region (F.E.B. and G in Fig. 2). The total anode current (of electron gun) I_A is kept to the $I_A = 0.3$ mA while the anode (electron gun) voltage V_A is varied. A bias voltage V_S for the beam collector B C. and the diffusional current collector D.C. is usually kept to $V_S = 200$V. (e): Electron Beam. (I_e): Electron Beam Current.

Fig. 3 Fringe magnetic field distribution.

B_M: Analyzing magnetic field of (M.A.). B_O: Uniform magnetic field inside (M.A.). X: End of uniform magnetic field. S: Entrance slit position. Fe: Magnetic field distribution in a case using iron plate as D in Fig. 1. Cu: Magnetic field distribution in a case using copper plate as D in Fig. 1.

Fig. 4 Applied electrical potential distribution.

V: Electrical potential. V_A: Initial potential (voltage) of electron gun anode. V_E Effective potential for μ^- (negative muonlike particle) and π^- (negative pionlike particle). e_0: Initial electrons from electron gun cathode. e_1: First electron beam. e_2: Second electron beam. i_1. Positive ion beam from plasma. i_2: Second positive ion beam. e–B: Electron bunch due to magnetic cyclotron motion. i–B: Positive ion bunch due to electrical retardation. K. Cathode position of electron gun. A: Anode position of electron gun. S: Slit position of mass analyzer. X: Entrance position of analyzing uniform magnetic field. $+V_A$ Additional potential generated by stopping the positive ion beam.

Fig 5 Dependences of negative (muonlike or pionlike particle) current Γ^- and electron current I_e to the beam collector B.C. on the mass analyzing magnetic field B_M.

(1): Γ^- at the first electron beam acceleration (electron gun anode) voltage $V_A = 100V$

(2): Γ^- at $V_A = 125V$. (3): Γ^- at $V_A = 150V$. (4): Γ^- at $V_A = 200V$. (5): Γ^- at $V_A = 400V$.

(1)': I_e at $V_A = 100V$. (2)': I_e at $V_A = 125V$. (5)': I_e at $V_A = 400V$.

Table 1 Comparisons between theoretical (typical) and experimental reduction ratios for μ^- or π^- peak of negative current Γ^-.

V_A : First electron acceleration voltage. α_1' (Th) or α_1' (Exp): Theoretical (Typical) or Experimental reduction ratio for μ^- peak of Γ^- from a case of $V_A = 400V$. α_2' (Th) or α_2' (Exp): Theoretical (Typical) or Experimental reduction ratio for π^- peak of Γ^- from a case of $V_A = 400V$.

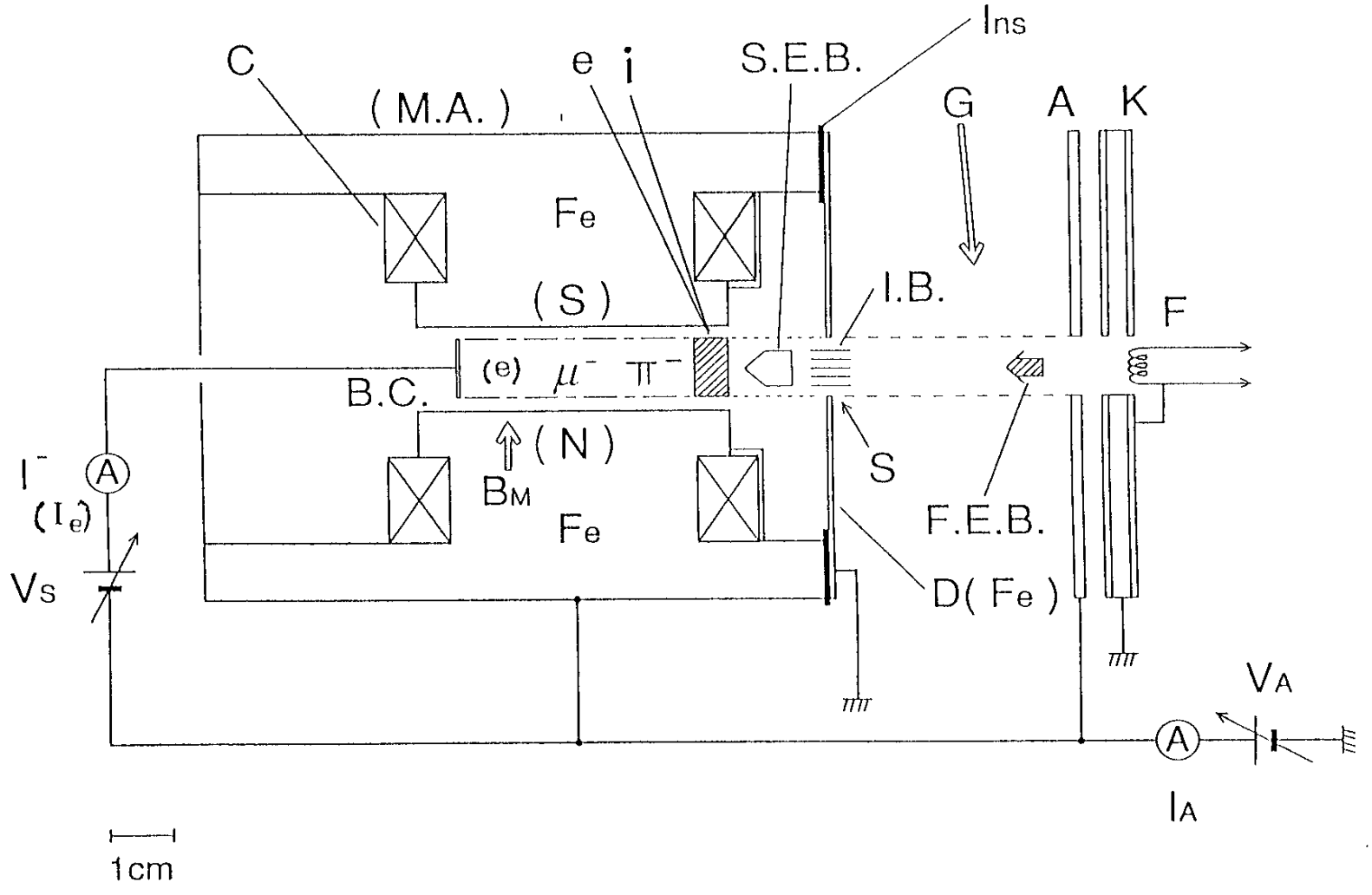
C
e
i
S.E.B.
Ins
(M.A.)
G
A
K
Fe
(S)
I.B.
F
(e) μ⁻ π⁻
B.C.
(N)
S
I⁻
(Ie)
A
BM
Fe
F.E.B.
D(Fe)
VS
VA
A
IA
1cm

Fig. 1

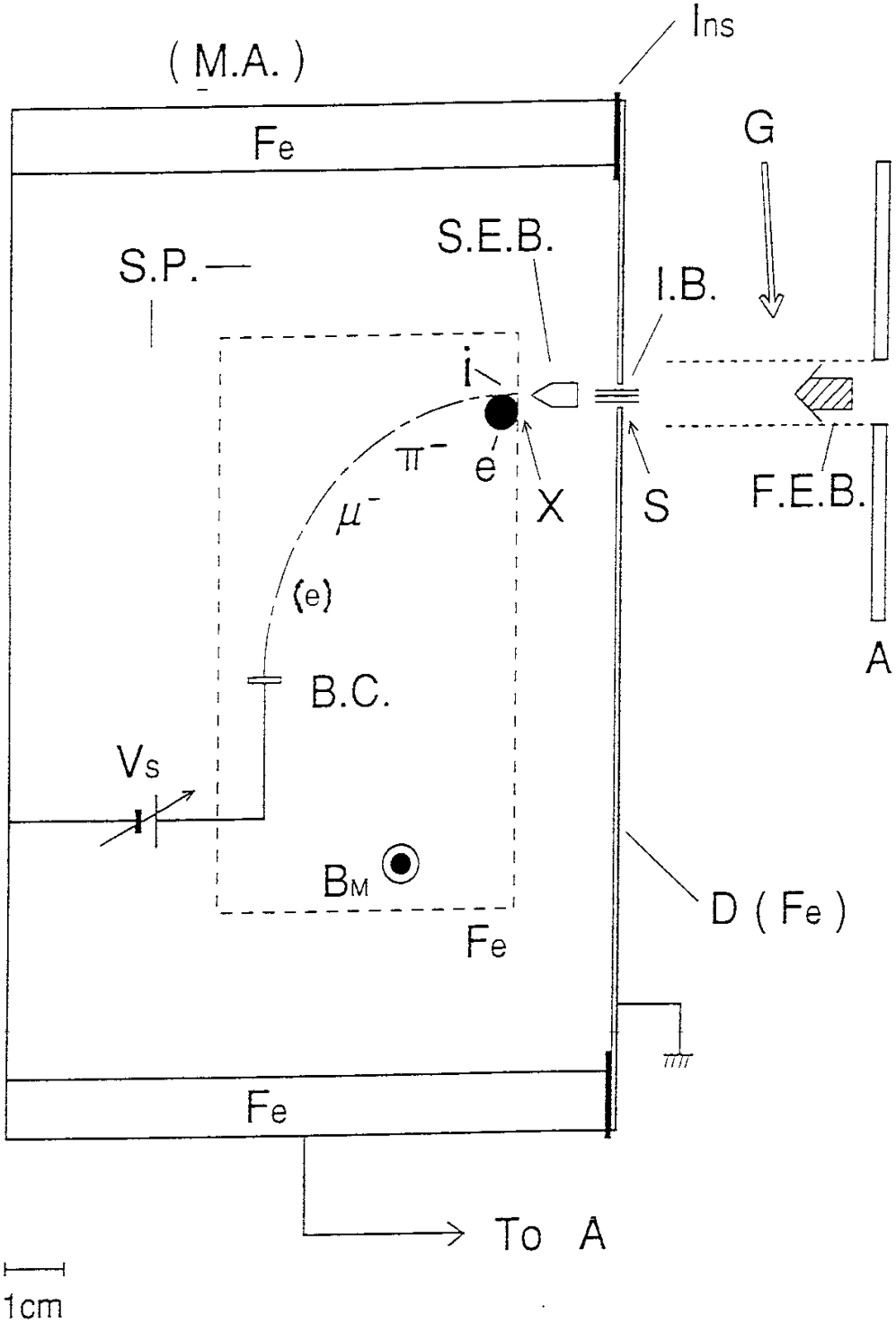

Fig. 2

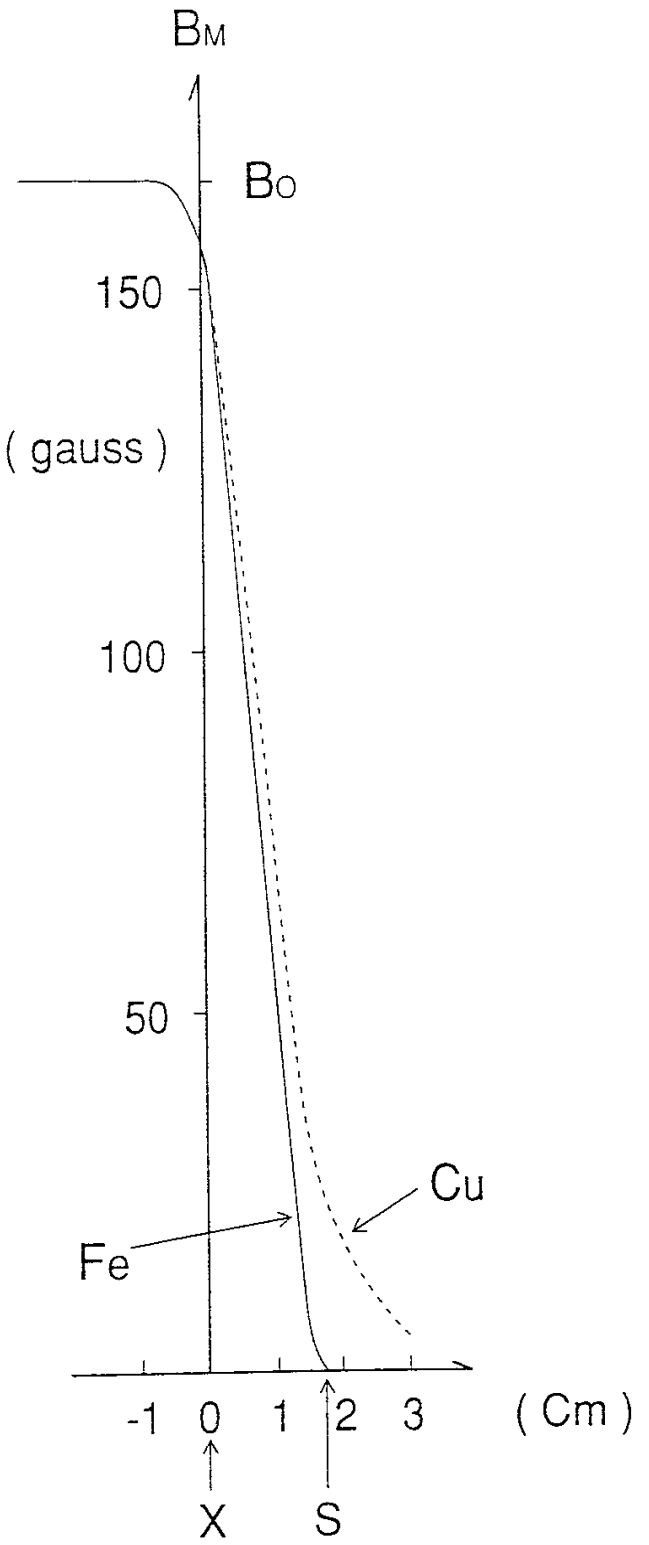

Fig. 3

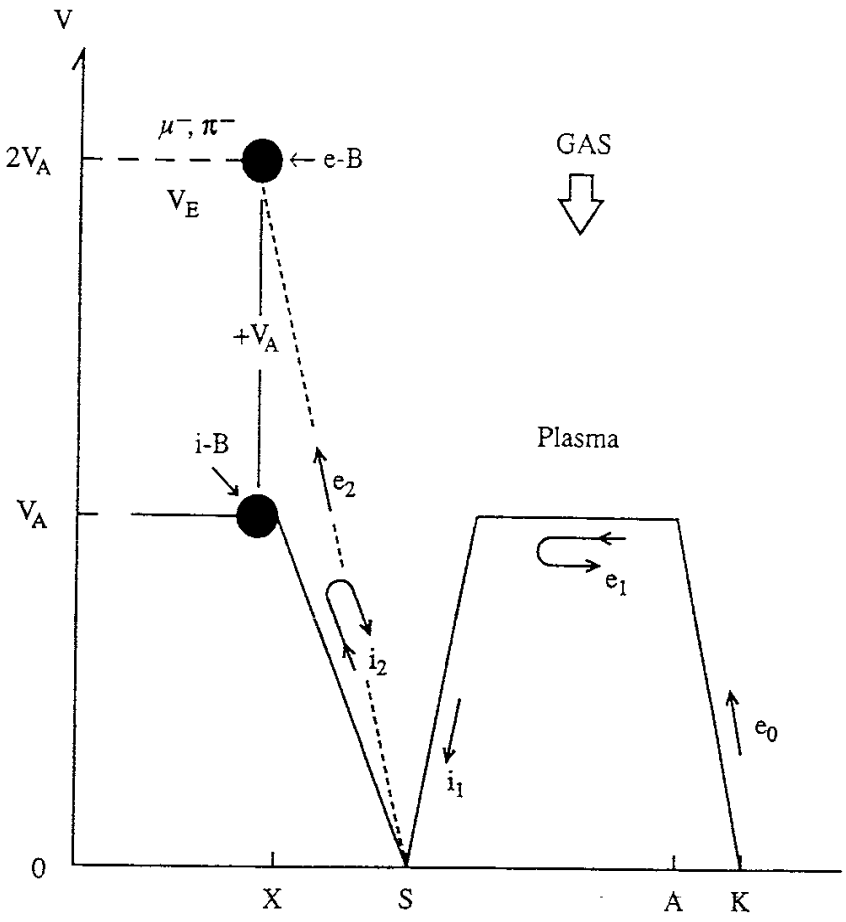

Fig. 4

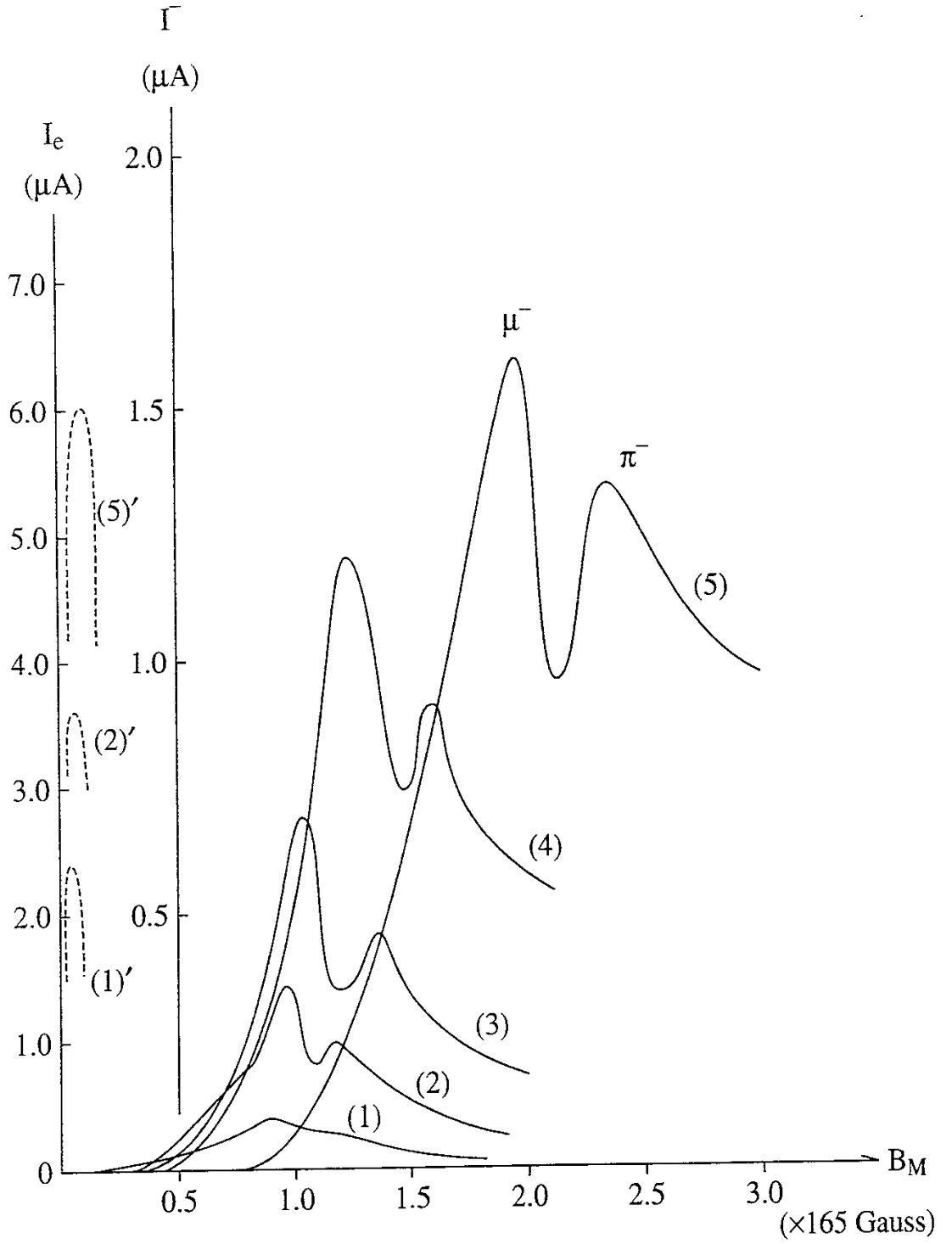
I⁻
(μA)
Ie
(μA)
2.0
7.0
6.0
1.5
5.0
4.0
1.0
3.0
2.0
0.5
1.0
0
μ⁻
π⁻
(5)′
(2)′
(1)′
(5)
(4)
(3)
(2)
(1)
0.5
1.0
1.5
2.0
2.5
3.0
BM
(×165 Gauss)

Fig. 5

		(5)	(4)	(3)	(2)	(1)
	V_A (V)	400	200	150	125	100
μ^-	α'_1 (Th)	1	$1/1.010$	$1/1.017$	$1/1.021$	$1/1.027$
	α'_1 (Exp)	1	$1/1.3$	$1/2.5$	$1/4.6$	$1/16$
π^-	α'_2 (Th)	1	$1/2.9$	$1/5.0$	$1/7.5$	$1/13$
	α'_2 (Exp)	1	$1/1.5$	$1/3.0$	$1/4.6$	$1/17$

Table 1

Recent Issues of NIFS Series

NIFS-304 K. Ida, H. Idei, H. Sanuki, K. Itoh, J. Xu, S. Hidekuma, K. Kondo, A. Sahara, H. Zushi, S.-I. Itoh, A. Fukuyama, K. Adati, R. Akiyama, S. Bessho, A. Ejiri, A. Fujisawa, M. Fujiwara, Y. Hamada, S. Hirokura, H. Iguchi, O. Kaneko, K. Kawahata, Y. Kawasumi, M. Kojima, S. Kubo, H. Kuramoto, A. Lazaros, R. Liang, K. Matsuoka, T. Minami, T. Mizuuchi, T. Morisaki, S. Morita, K. Nagasaki, K. Narihara, K. Nishimura, A. Nishizawa, T. Obiki, H. Okada, S. Okamura, T. Ozaki, S. Sakakibara, H. Sakakita, A. Sagara, F. Sano, M. Sasao, K. Sato, K.N. Sato, T. Saeki, S. Sudo, C. Takahashi, K. Tanaka, K. Tsumori, H.Yamada, I. Yamada, Y. Takita, T. Tuzuki, K. Toi and T. Watari, *Control of Radial Electric Field in Torus Plasma;* Sep. 1994 (IAEA-CN-60/A-2-IV-2)

NIFS-305 T. Hayashi, T. Sato, N. Nakajima, K. Ichiguchi, P. Merkel, J. Nührenberg, U. Schwenn, H. Gardner, A. Bhattacharjee and C.C.Hegna, *Behavior of Magnetic Islands in 3D MHD Equilibria of Helical Devices*; Sep. 1994 (IAEA-CN-60/D-2-II-4)

NIFS-306 S. Murakami, M. Okamoto, N. Nakajima, K.Y. Watanabe, T. Watari, T. Mutoh, R. Kumazawa and T. Seki, *Monte Carlo Simulation for ICRF Heating in Heliotron/Torsatrons*; Sep. 1994 (IAEA-CN-60/D-P-I-14)

NIFS-307 Y. Takeiri, A. Ando, O. Kaneko, Y. Oka, K. Tsumori, R. Akiyama, E. Asano, T. Kawamoto, T. Kuroda, M. Tanaka and H. Kawakami, *Development of an Intense Negative Hydrogen Ion Source with a Wide-Range of External Magnetic Filter Field*; Sep. 1994

NIFS-308 T. Hayashi, T. Sato, H.J. Gardner and J.D. Meiss, *Evolution of Magnetic Islands in a Heliac*; Sep. 1994

NIFS-309 H. Amo, T. Sato and A. Kageyama, *Intermittent Energy Bursts and Recurrent Topological Change of a Twisting Magnetic Flux Tube*; Sep.1994

NIFS-310 T. Yamagishi and H. Sanuki, *Effect of Anomalous Plasma Transport on Radial Electric Field in Torsatron/Heliotron*; Sep. 1994

NIFS-311 K. Watanabe, T. Sato and Y. Nakayama, *Current-profile Flattening and Hot Core Shift due to the Nonlinear Development of Resistive Kink Mode*; Oct. 1994

NIFS-312 M. Salimullah, B. Dasgupta, K. Watanabe and T. Sato, *Modification and Damping of Alfvén Waves in a Magnetized Dusty Plasma*; Oct. 1994

NIFS-313 K. Ida, Y. Miura, S -I. Itoh, J.V. Hofmann, A. Fukuyama, S. Hidekuma, H. Sanuki, H. Idei, H. Yamada, H. Iguchi, K. Itoh,
Physical Mechanism Determining the Radial Electric Field and its Radial Structure in a Toroidal Plasma; Oct. 1994

NIFS-314 Shao-ping Zhu, R. Horiuchi, T. Sato and The Complexity Simulation Group,
Non-Taylor Magnetohydrodynamic Self-Organization; Oct. 1994

NIFS-315 M. Tanaka,
Collisionless Magnetic Reconnection Associated with Coalescence of Flux Bundles; Nov. 1994

NIFS-316 M. Tanaka,
Macro-EM Particle Simulation Method and A Study of Collisionless Magnetic Reconnection; Nov. 1994

NIFS-317 A. Fujisawa, H. Iguchi, M. Sasao and Y. Hamada,
Second Order Focusing Property of 210° Cylindrical Energy Analyzer; Nov. 1994

NIFS-318 T. Sato and Complexity Simulation Group,
Complexity in Plasma - A Grand View of Self- Organization; Nov. 1994

NIFS-319 Y. Todo, T. Sato, K. Watanabe, T.H. Watanabe and R. Horiuchi,
MHD-Vlasov Simulation of the Toroidal Alfvén Eigenmode; Nov. 1994

NIFS-320 A. Kageyama, T. Sato and The Complexity Simulation Group,
Computer Simulation of a Magnetohydrodynamic Dynamo II: Nov. 1994

NIFS-321 A. Bhattacharjee, T. Hayashi, C.C.Hegna, N. Nakajima and T. Sato,
Theory of Pressure-induced Islands and Self-healing in Three-dimensional Toroidal Magnetohydrodynamic Equilibria; Nov. 1994

NIFS-322 A. Iiyoshi, K. Yamazaki and the LHD Group,
Recent Studies of the Large Helical Device; Nov. 1994

NIFS-323 A. Iiyoshi and K. Yamazaki,
The Next Large Helical Devices; Nov. 1994

NIFS-324 V.D. Pustovitov
Quasisymmetry Equations for Conventional Stellarators; Nov. 1994

NIFS-325 A. Taniike, M. Sasao, Y. Hamada, J. Fujita, M. Wada,
The Energy Broadening Resulting from Electron Stripping Process of a Low Energy Au^- Beam; Dec. 1994

NIFS-326 I. Viniar and S. Sudo,
New Pellet Production and Acceleration Technologies for High Speed Pellet Injection System "HIPEL" in Large Helical Device; Dec. 1994

NIFS-327 Y. Hamada, A. Nishizawa, Y. Kawasumi, K. Kawahata, K. Itoh, A. Ejiri, K. Toi, K. Narihara, K. Sato, T. Seki, H. Iguchi, A. Fujisawa, K. Adachi, S. Hidekuma, S. Hirokura, K. Ida, M. Kojima, J. Koong, R. Kumazawa, H. Kuramoto, R. Liang, T. Minami, H. Sakakita, M. Sasao, K.N. Sato, T. Tsuzuki, J. Xu, I. Yamada, T. Watari,
Fast Potential Change in Sawteeth in JIPP T-IIU Tokamak Plasmas; Dec. 1994

NIFS-328 V.D. Pustovitov,
Effect of Satellite Helical Harmonics on the Stellarator Configuration; Dec. 1994

NIFS-329 K. Itoh, S-I. Itoh and A. Fukuyama,
A Model of Sawtooth Based on the Transport Catastrophe; Dec. 1994

NIFS-330 K. Nagasaki, A. Ejiri,
Launching Conditions for Electron Cyclotron Heating in a Sheared Magnetic Field; Jan. 1995

NIFS-331 T.H. Watanabe, Y. Todo, R. Horiuchi, K. Watanabe, T. Sato,
An Advanced Electrostatic Particle Simulation Algorithm for Implicit Time Integration; Jan. 1995

NIFS-332 N. Bekki and T. Karakisawa,
Bifurcations from Periodic Solution in a Simplified Model of Two-dimensional Magnetoconvection; Jan. 1995

NIFS-333 K. Itoh, S.-I. Itoh, M. Yagi, A. Fukuyama,
Theory of Anomalous Transport in Reverse Field Pinch; Jan. 1995

NIFS-334 K. Nagasaki, A. Isayama and A. Ejiri
Application of Grating Polarizer to 106.4GHz ECH System on Heliotron-E; Jan. 1995

NIFS-335 H. Takamaru, T. Sato, R. Horiuchi, K. Watanabe and Complexity Simulation Group,
A Self-Consistent Open Boundary Model for Particle Simulation in Plasmas; Feb. 1995

NIFS-336 B.B. Kadomtsev,
Quantum Telegragh : is it possible?; Feb. 1995

NIFS-337 B.B.Kadomtsev,
Ball Lightning as Self-Organization Phenomenon; Feb. 1995

NIFS-338 Y. Takeiri, A. Ando, O. Kaneko, Y. Oka, K. Tsumori, R. Akiyama, E. Asano, T. Kawamoto, M. Tanaka and T. Kuroda,
High-Energy Acceleration of an Intense Negative Ion Beam; Feb. 1995

NIFS-339 K. Toi, T. Morisaki, S. Sakakibara, S. Ohdachi, T.Minami, S. Morita, H. Yamada, K. Tanaka, K. Ida, S. Okamura, A. Ejiri, H. Iguchi, K. Nishimura, K. Matsuoka, A. Ando, J. Xu, I. Yamada, K. Narihara, R. Akiyama, H. Idei, S. Kubo, T. Ozaki, C. Takahashi, K. Tsumori, *H-Mode Study in CHS*; Feb. 1995

NIFS-340 T. Okada and H. Tazawa, *Filamentation Instability in a Light Ion Beam-plasma System with External Magnetic Field*; Feb. 1995

NIFS-341 T. Watanbe, G. Gnudi, *A New Algorithm for Differential-Algebraic Equations Based on HIDM*; Feb. 13, 1995

NIFS-342 Y. Nejoh, *New Stationary Solutions of the Nonlinear Drift Wave Equation;* Feb. 1995

NIFS-343 A. Ejiri, S. Sakakibara and K. Kawahata, *Signal Based Mixing Analysis for the Magnetohydrodynamic Mode Reconstruction from Homodyne Microwave Reflectometry*; Mar.. 1995

NIFS-344 B.B.Kadomtsev, K. Itoh, S.-I. Itoh *Fast Change in Core Transport after L-H Transition*; Mar. 1995

NIFS-345 W.X. Wang, M. Okamoto, N. Nakajima and S. Murakami, *An Accurate Nonlinear Monte Carlo Collision Operator*; Mar. 1995

NIFS-346 S. Sasaki, S. Takamura, S. Masuzaki, S. Watanabe, T. Kato, K. Kadota, *Helium I Line Intensity Ratios in a Plasma for the Diagnostics of Fusion Edge Plasmas*; Mar. 1995

NIFS-347 M. Osakabe, *Measurement of Neutron Energy on D-T Fusion Plasma Experiments;* Apr. 1995

NIFS-348 M. Sita Janaki, M.R. Gupta and Brahmananda Dasgupta, *Adiabatic Electron Acceleration in a Cnoidal Wave;* Apr. 1995

NIFS-349 J. Xu, K. Ida and J. Fujita, *A Note for Pitch Angle Measurement of Magnetic Field in a Toroidal Plasma Using Motional Stark Effect*; Apr. 1995

NIFS-350 J. Uramoto, *Characteristics for Metal Plate Penetration of a Low Energy Negative Muonlike or Pionlike Particle Beam*: Apr. 1995